Synaptic Transmission at PNS: the **Neuromuscular Junction**

1. The Synaptogenesis
2. The Synaptic Transmission at NMJ
3. The Safety Factor
4. Myasthenic Syndromes
5. **The Tripartite Synapse**

Presynaptic membrane senses the ACh by both nAChR and mAChR

Postsynaptic ….

What about PSCs?

EXPERIMENTAL NEUROLOGY **88,** 198–204 (1985)

On the Brain of a Scientist: Albert Einstein

MARIAN C. DIAMOND,* ARNOLD B. SCHEIBEL,†
GREER M. MURPHY, JR.,‡ AND THOMAS HARVEY[1]

**Departments of Physiology–Anatomy and ‡Anthropology, University of California, Berkeley, California 94720, and †Departments of Anatomy and Psychiatry, University of California, Los Angeles, California 90024*

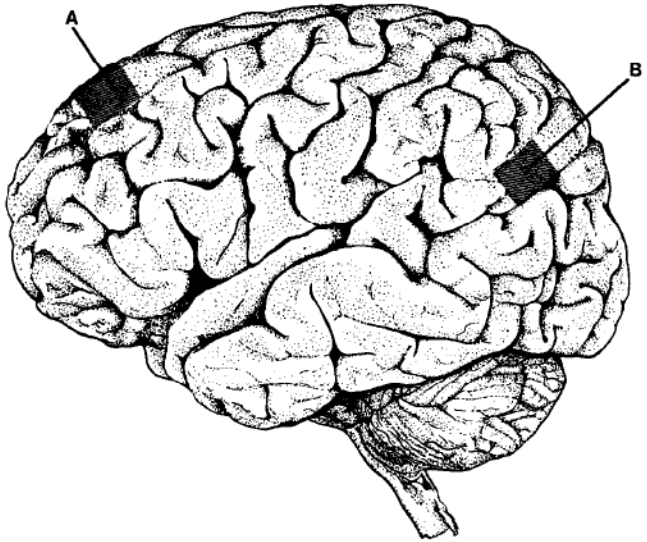

FIG. 1. A lateral view of the human brain indicating the position of the samples removed for cell counts. A represents the sample from area 9 and B, area 39.

TABLE 1

Neuron:Glial Ratios between Einstein's Brain and Those from 11 Males (47 to 80 Years of Age)

Region	$N:G_{\bar{x}}$ (11 males)	SD	$N:G_{\bar{x}}$[a] Einstein	% Δ	*P*
Left area 9	1.849	0.661	1.04	77	NS
Right area 9	1.754	0.755	1.16	51	NS
Left area 39	1.936	0.312	1.12	73	0.05
Right area 39	2.026	0.588	0.92	120	NS

[a] In every area Einstein had a smaller N:G ratio, but by comparing one brain with 11 having relatively large SDs, the results showed only one area to be significantly different.

The tripartite synapse

at the central nervous system

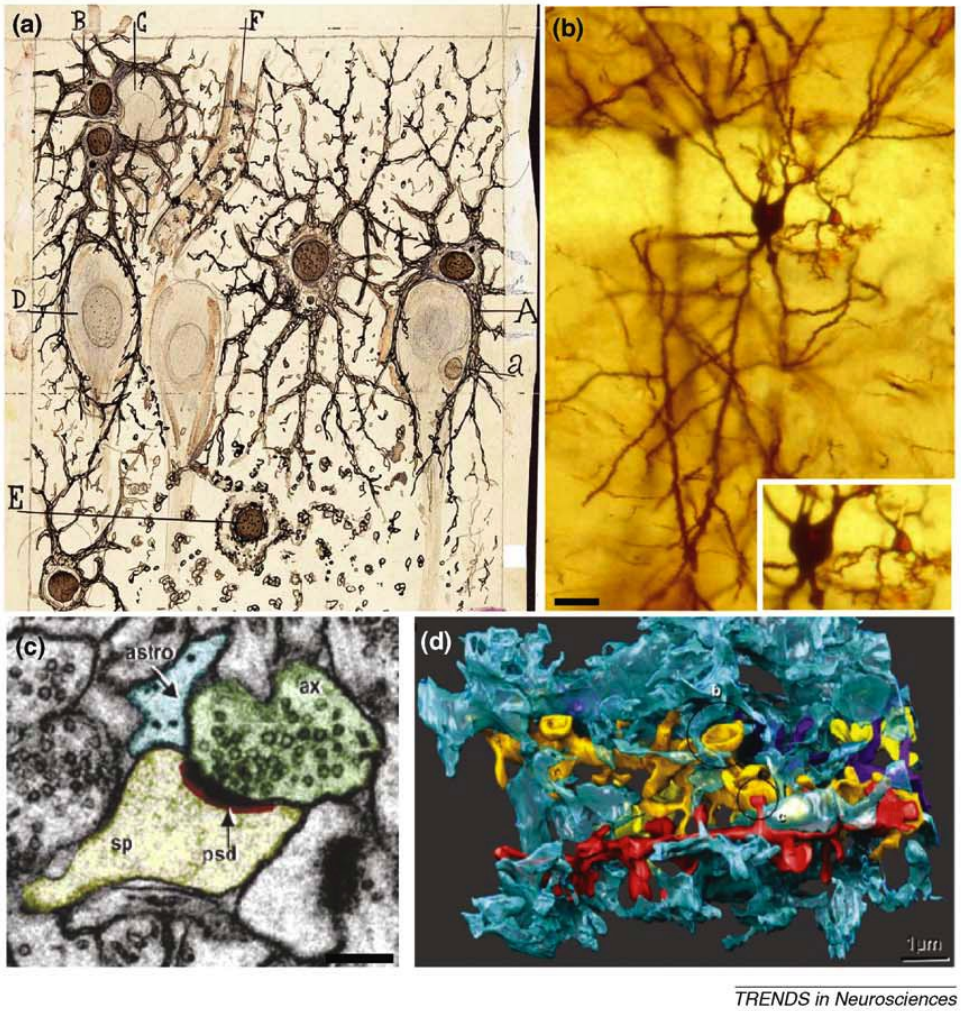

TRENDS in Neurosciences

Tripartite synapses: glia, the unacknowledged partner

Alfonso Araque, Vladimir Parpura, Rita P. Sanzgiri and Philip G. Haydon

TINS Vol. 22, No. 5, 1999

Tripartite synapses: astrocytes process and control synaptic information

Gertrudis Perea, Marta Navarrete and Alfonso Araque

Instituto Cajal, Consejo Superior de Investigaciones Científicas, Madrid 28002, Spain

Trends in Neurosciences Vol.32 No.8

The coverage domain
of a single astrocyte is between
20,000-140,000 synapses in rodent
hippocampus and 250,000-2 millions
in human!

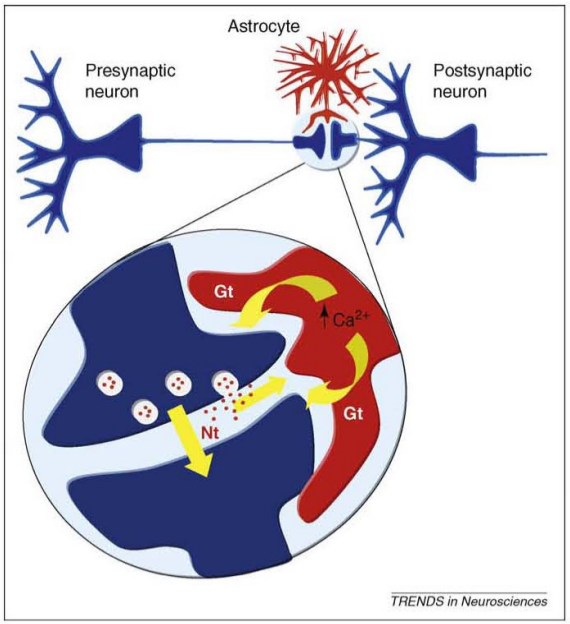

Figure 2. Scheme of the tripartite synapse. Cartoon representing the transfer of information between neuronal elements and astrocyte at the tripartite synapse. Astrocytes respond with Ca^{2+} elevations to neurotransmitters (Nt) released during synaptic activity and, in turn, control neuronal excitability and synaptic transmission through the Ca^{2+}-dependent release of gliotransmitters (Gt).

* If we also include microglial processes and the extracellular matrix (ECM), the tripartite paradigm can be uploaded to tetra or pentapartite synapse.

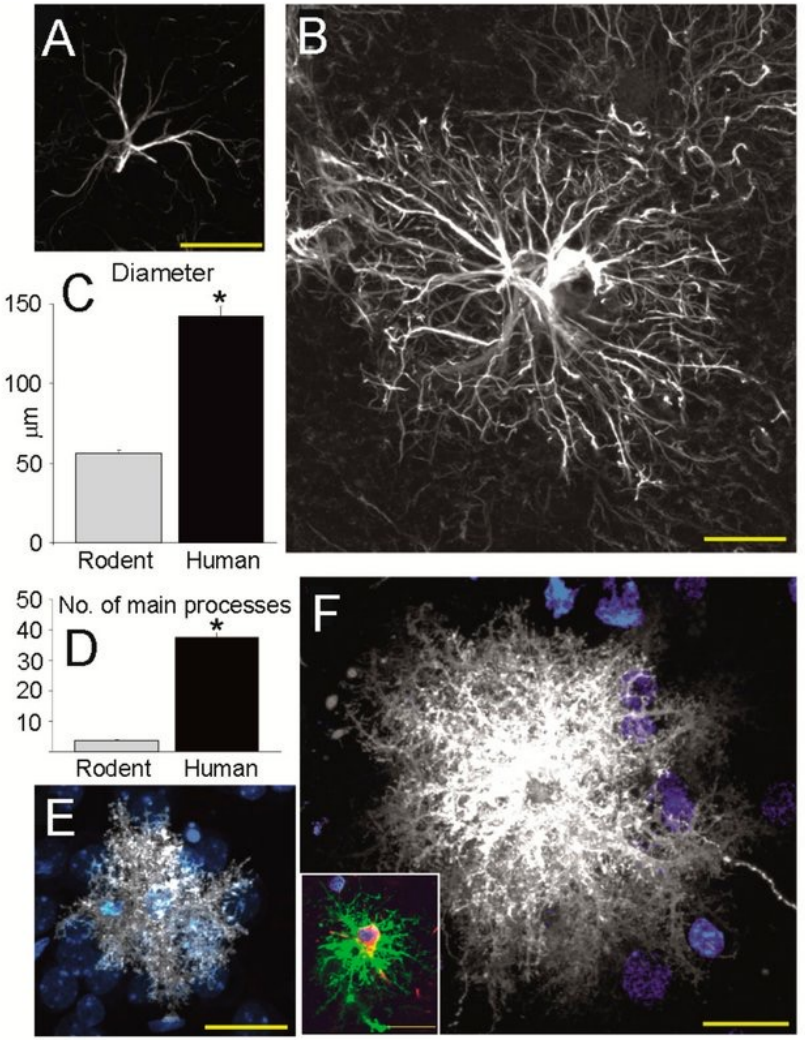

Figure 3. Comparison of rodent and human protoplasmic astrocytes. (A) Typical mouse protoplasmic astrocyte. Glial fibrillary acidic protein (GFAP) staining is shown in white. Scale bar: 20 µm. (B) Typical human protoplasmic astrocyte in the same scale. Scale bar: 20 µm. (C,D) Human protoplasmic astrocytes are 2.55-fold larger and have 10-fold more main GFAP processes than mouse astrocytes (human, n = 50 cells from seven patients; mouse, n = 65 cells from six mice; mean ± standard error mean (SEM); *$p < 0.005$, t-test). (E) Mouse protoplasmic astrocyte diolistically labelled with lypophilic dye DiI (white staining) and sytox (blue staining) revealing the full structure of the astrocyte, including its numerous fine processes. Scale bar: 20 µm. (F) Diolistically-labelled human astrocyte demonstrates the highly complicated network of fine process that defines the human protoplasmic astrocyte. Scale bar: 20 µm. Inset: Diolistically-labelled human protoplasmic astrocyte, also immunolabelled for GFAP (green staining), demonstrating colocalization. Scale bar: 20 µm. Reproduced with permission from [50].

Table 1. Ca^{2+} signaling in astrocytes

	Neurotransmitter	Experimental model	Brain area	Refs
Spontaneous activity	Non-applicable	Brain slices	Thalamus	[12,14]
			Hippocampus	[12,13]
			Cerebellum	[12,24]
			Cortex	[15]
			Striatum	[12]
		In vivo	Cortex	[31,32,34–36]
Synaptically evoked	Norepinephrine	Brain slices	Cerebellum	[19]
		In vivo	Cortex	[34]
	ATP	Brain slices	Hippocampus	[81]
			Cerebellum	[82,83]
			Retina	[84]
			Olfatory bulb	[85]
	GABA	Brain slices	Hippocampus	[18,70]
	Glutamate	Brain slices	Hippocampus	[16,17,20,25,86]
			Cortex	[20,39]
			Nucleus accumbens	[61]
			Cerebellum	[82,83]
			Olfatory Bulb	[85]
		In vivo	Cortex	[33,37]
	Acetylcholine	Brain slices	Hippocampus	[16,25]
	Nitric Oxide	Brain slices	Cerebellum	[87]
	Endocannabinoids	Brain slices	Hippocampus	[64]

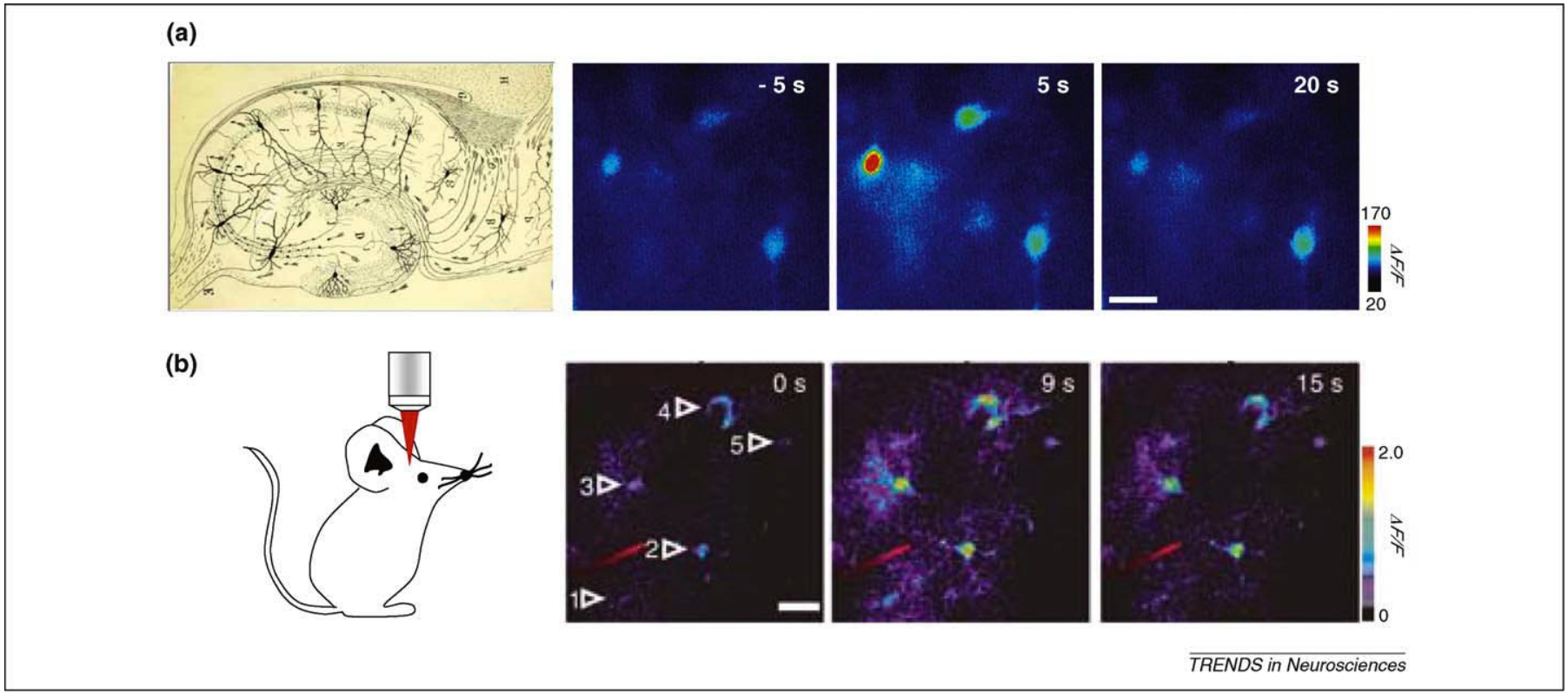

Figure 3. Astrocyte Ca2+ signaling in brain slices and in vivo. (a) Cajal's drawing of the mammalian hippocampus (reproduced from an original drawing with permission of the Instituto Cajal) and pseudocolor images from rat hippocampal slices representing fluorescence intensities indicative of astrocyte Ca2+ levels before (5 s) and after (5 s, 20 s) electrical stimulation of Schaffer collaterals. Scale bar, 10 mm. (b) Two-photon microscopy images of the in vivo astrocyte Ca2+ signal in the barrel cortex. Pseudocolor images represent fluorescence intensities indicative of astrocyte Ca2+ levels before (0 s) and after (9 s, 15 s) evoked by whisker stimulation. Scale bar, 20 mm. Reproduced, with permission, from Ref. [33]. Note the astrocyte Ca2+ elevations evoked by electrical synaptic and sensory stimulation in hippocampal slices (a) and in vivo barrel cortex b), respectively.

Astrocytes integrate synaptic information

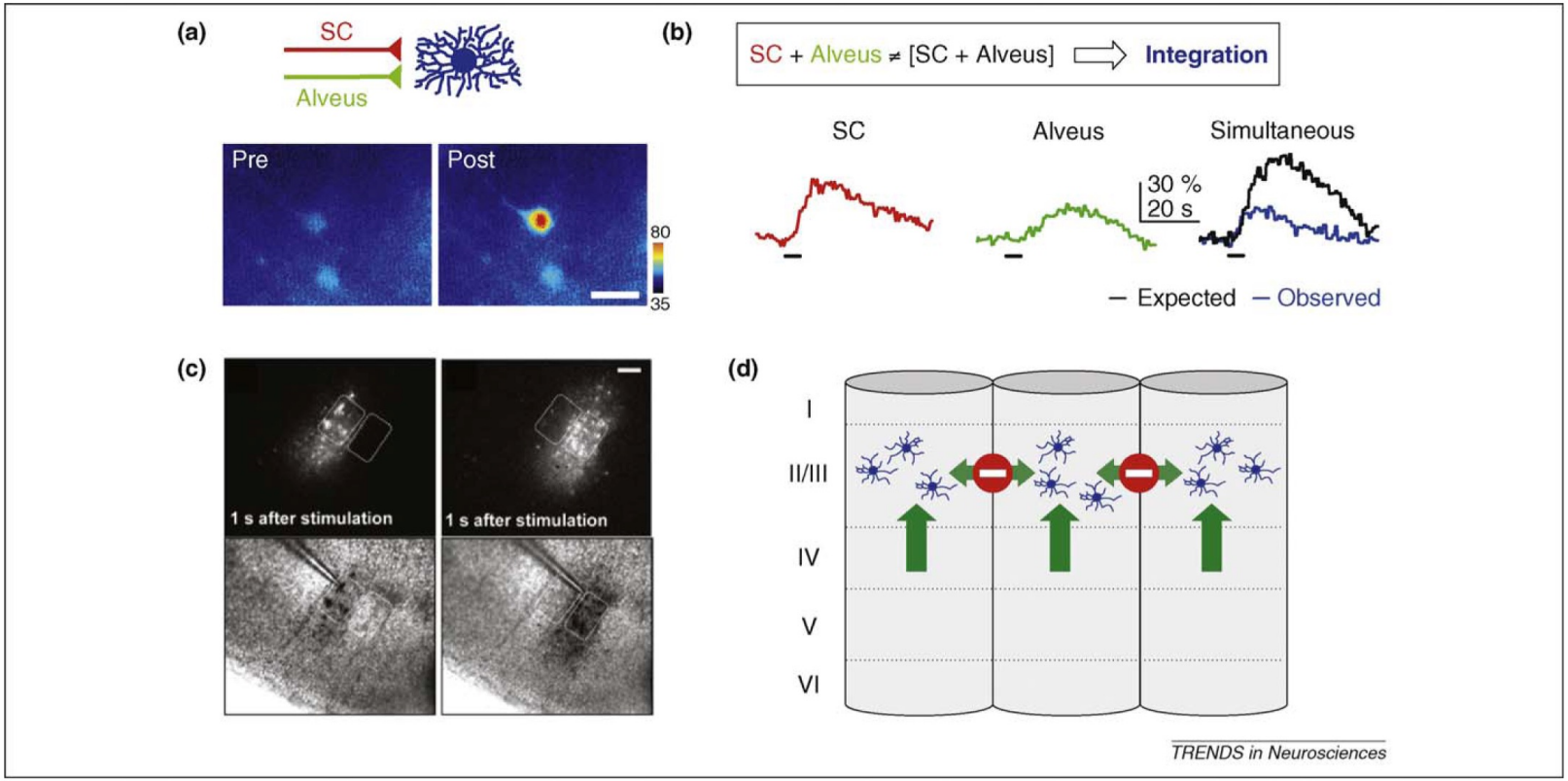

Alveus: GLU & ACh

SC: GLU

Figure 4. Astrocytes integrate synaptic information. **(a)** Schematic drawing and pseudocolor images of astrocyte Ca^{2+} elevations evoked by stimulation of Schaffer collaterals (SC, red) or alveus (green). Astrocytes integrate synaptic information from different synaptic inputs. Scale bar, 15 μm. **(b)** Hypothesis of astrocyte integration of synaptic information induced by SC and alveus activity (top) and astrocyte Ca^{2+} signals evoked by independent and simultaneous stimulation of SC and alveus (bottom). Blue and black traces correspond to the observed and expected responses (i.e. the linear summation of the responses evoked by independent stimulation of both pathways), respectively. Horizontal lines at the bottom of each trace represent the stimuli. Modified from Ref. [25]. Note the lack of correspondence between observed and expected responses, that is, the relative reduction of the observed response versus the linear summation of the responses evoked independently, which is indicative of synaptic integration. **(c)** Top, fluorescence images showing astrocytic Ca^{2+} signals evoked after electrical stimulation (responding cells are displayed in white) of two contiguous barrel cortex. Bottom, images showing an overlay of the bright-field image with the location of the stimulating pipette and the responding astrocytes (shown in black). The barrels in layer 4 are outlined by dotted white lines. Scale bar, 100 μm. Note that astrocytes that respond to the stimulation of the barrel column are located within the stimulated barrel column, and no astrocytes respond to the stimulation of the adjacent barrel column, which indicates the selectivity of astrocyte responses. Reproduced, with permission, from Ref. [39]. **(d)** Schematic drawing illustrating the discrimination and response selectivity of barrel cortex astrocytes to neuronal activity from layer IV but not from layer II/III of neighboring barrels.

Astrocytes regulate neuronal activity

Table 2. Gliotransmitters and synaptic transmission

Gliotransmitter	Experimental preparation	Neuromodulation	Refs
Glutamate	Hippocampus	Depression of evoked EPSCs and IPSCs	[43,67]
		Frequency increase of miniature PSCs	[44]
		Frequency increase of miniature IPSCs	[18]
		Frequency increase of spontaneous EPSCs	[50,26]
		Frequency increase of spontaneous IPSCs	[66]
		Postsynaptic SIC	[25,43,60,62,64,65,88–94]
		Increase of neuronal excitability	[17]
		Heterosynaptic depression	[95]
	Cortex	Postsynaptic SIC	[96]
	Ventro basal thalamus	Postsynaptic SIC	[14]
	Nucleus accumbens	Postsynaptic SIC	[61]
	Olfactory Bulb	Postsynaptic SIC	[63]
	Retina	Light-evoked neuronal activity	[97]
ATP/Adenosine	Cerebellum	Depression of spontaneous EPSCs	[98]
	Hippocampus	Heterosynaptic depresion of EPSCs	[70,71]
		Modulation of LTP	[69]
		Synaptic depression	[69]
	Hypothalamic paraventricular nucleus	Insertion of AMPA receptors	[99]
	Retina	Depression of light-evoked EPSCs	[100]
D-Serine	Hippocampus	Modulation of LTP	[101]
	Hipothalamic supraoptic Nucleus	Modulation of LTP	[72]
	Retina	Potentiate NMDA receptor transmission	[102]
TNFα	Hippocampus	Insertion of AMPA receptors	[74]
		Increase of synaptic scaling	[76]
GABA	Olfactory bulb	Postsynaptic SOC	[63]
Undefined (glutamate and/or nitric oxide)	Neuromuscular junction	Synaptic depression	[103,104]
		Synaptic potentiation	[105]

Abbreviations: EPSCs, excitatory postsynaptic currents; IPSCs, inhibitory postsynaptic currents; LTP, long-term potentiation; PSCs, postsynaptic currents; SIC, slow inward current; SOC, slow outward current.

The gliotransmitter release

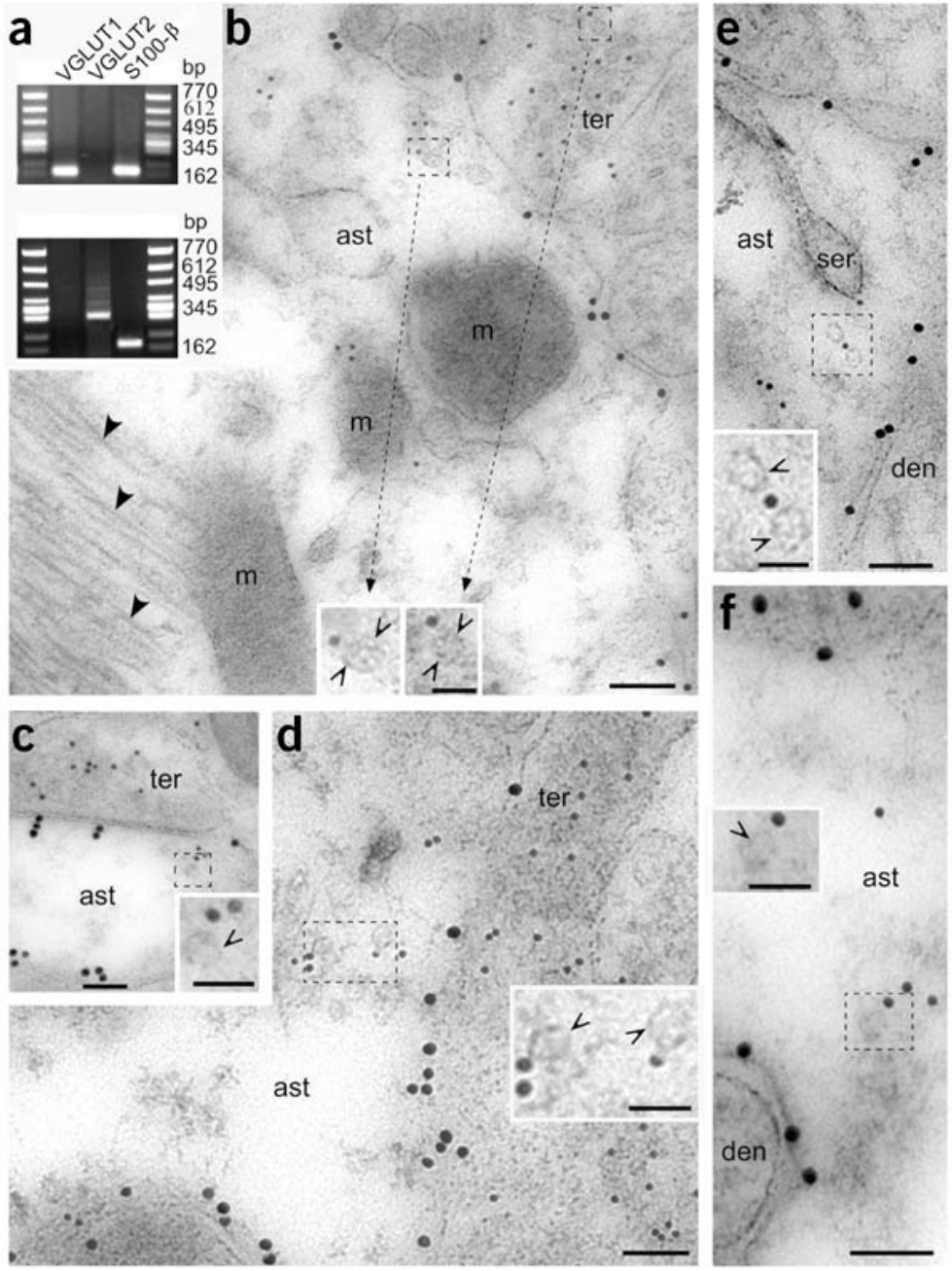

Figure 1. VGLUT-positive small vesicular organelles in astrocytic processes that face neuronal structures in the hippocampus.
(a) cDNA gels from electrophysiologically identified astrocytes of the outer molecular layer of the hippocampal dentate gyrus show the coexpression of the astrocyte marker S100beta (175 bp) and VGLUT1 (165 bp, upper gel) or VGLUT2 (286 bp, lower gel). (b–f) Electron micrographs of (b–e) VGLUT1 and (f) VGLUT2 (small gold particles) in astrocyte processes in the molecular layers of the dentate gyrus. The astrocyte processes are identified by labeling for GLT/GLAST25 (large gold particles) and by the presence of filaments (filled arrowheads). In b, VGLUT1 is located in small groups over vesicular organelles in an astrocyte process (ast) close to the plasma membrane facing a VGLUT1-positive nerve terminal (ter). Insets: Higher magnifications highlighting the similar appearance of VGLUT1-positive vesicles in astrocytes and in nerve terminals (open arrowheads). m, mitochondria. Other examples of VGLUT1-positive vesicles are shown in c and d, just beneath the plasma membrane that opposes VGLUT1-positive nerve terminals (ter). Insets: Higher magnifications showing the astrocyte vesicles (open arrowheads) labeled for VGLUT1. In e, VGLUT1-positive vesicular organelles are close to a tubular structure resembling smooth endoplasmatic reticulum (ser). Inset: Higher magnification showing a VGLUT1 gold particle belonging to either of the vesicles (open arrowheads). den, dendrite. (f) VGLUT2 labeling in an astrocyte process. Inset: A vesicular organelle (open arrowhead) is positive for VGLUT2. den, dendrite. Scale bars, 100 nm in b–f and 50 nm in insets.

Li et al. J Neurosci. 2013 6;33(10):4434-55.

The Schwann cells

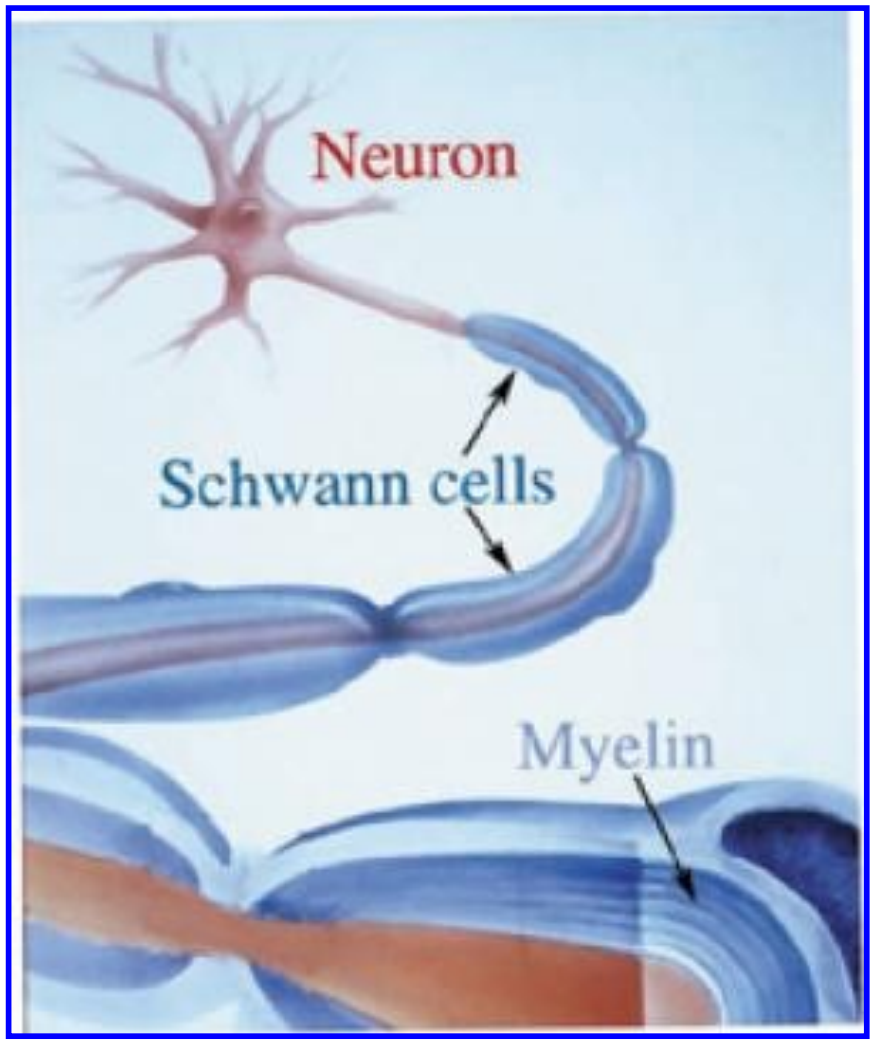

Ensheath axons, forming myelin, and allowing fast propagation of action potential.

Terminal Schwann Cells (TSC), also known as Perisynaptic Schwann Cells (PSC) are located in PNS

Definition: any Nonmyelinating Schwann Cell associated with an axon terminal, regardless of end-organ structure (e.g. somatosensory and somatic motor systems).

They are involved in:

synaptic development, facilitating and maintaining neural transmission

repairing damage following injury

They **sense neurotransmission**, releasing cytokines, influencing synaptic competition, and removing supernumerary axons. They are also involved in diseases and aging.

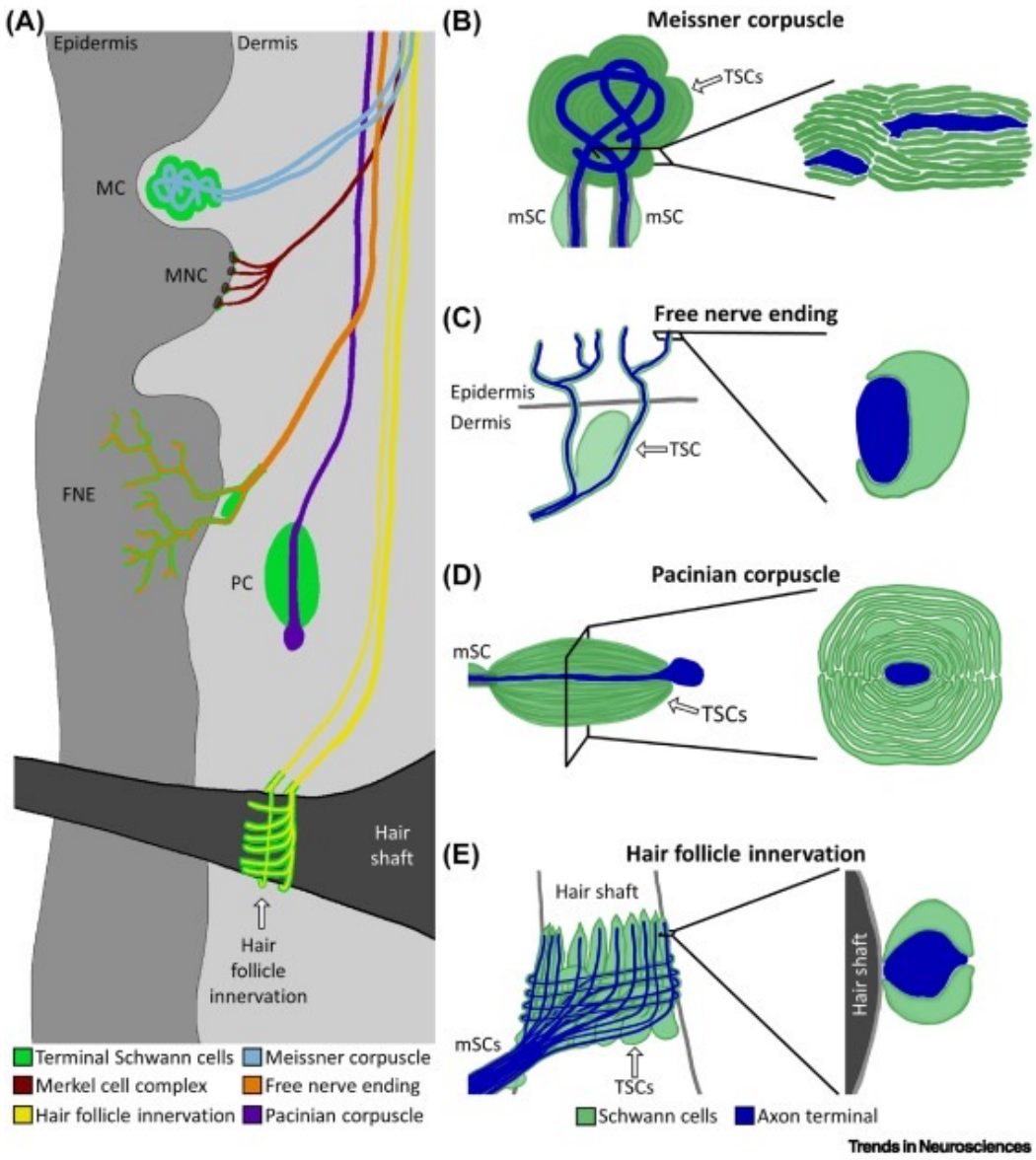

The Tripartite Synapse

At the central nervous system

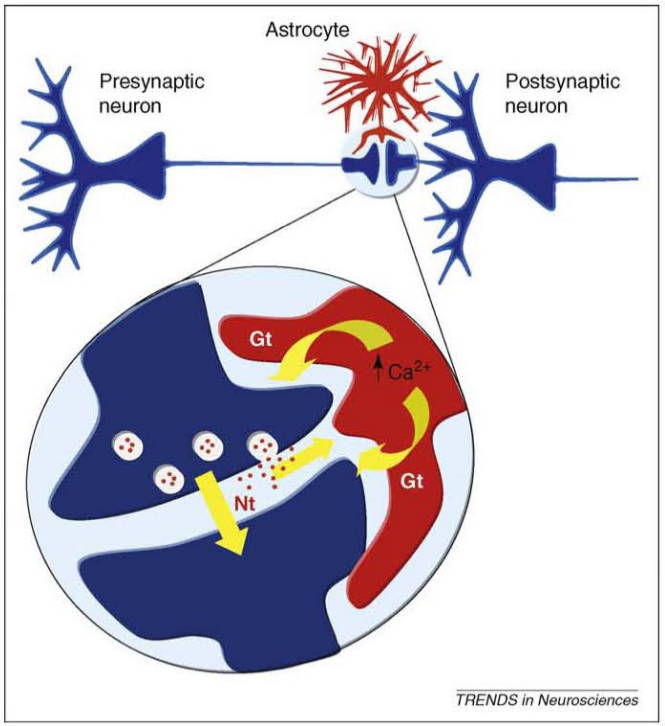

Figure 2. Scheme of the tripartite synapse. Cartoon representing the transfer of information between neuronal elements and astrocyte at the tripartite synapse. Astrocytes respond with Ca^{2+} elevations to neurotransmitters (Nt) released during synaptic activity and, in turn, control neuronal excitability and synaptic transmission through the Ca^{2+}-dependent release of gliotransmitters (Gt).

At the peripheral nervous system

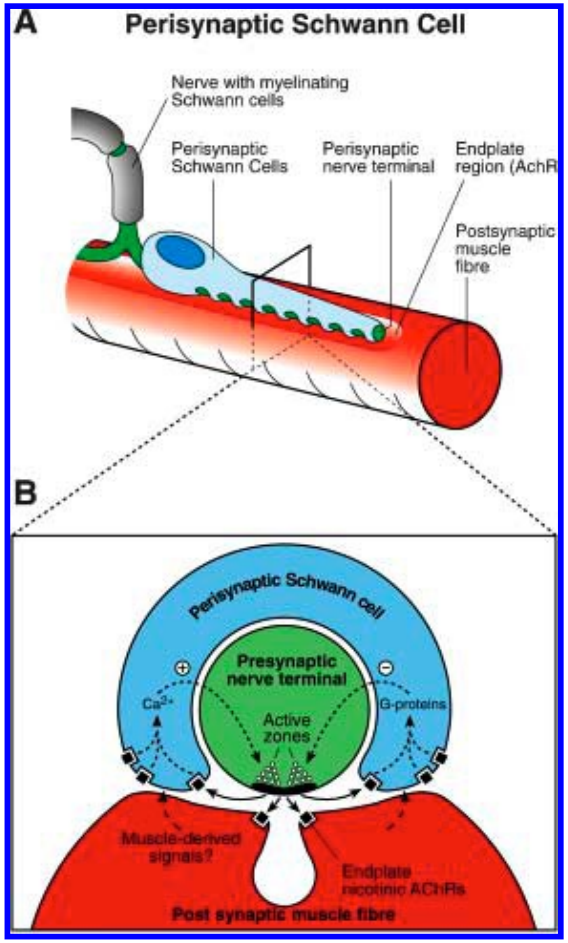

The TSCs
sense the synaptic
activity

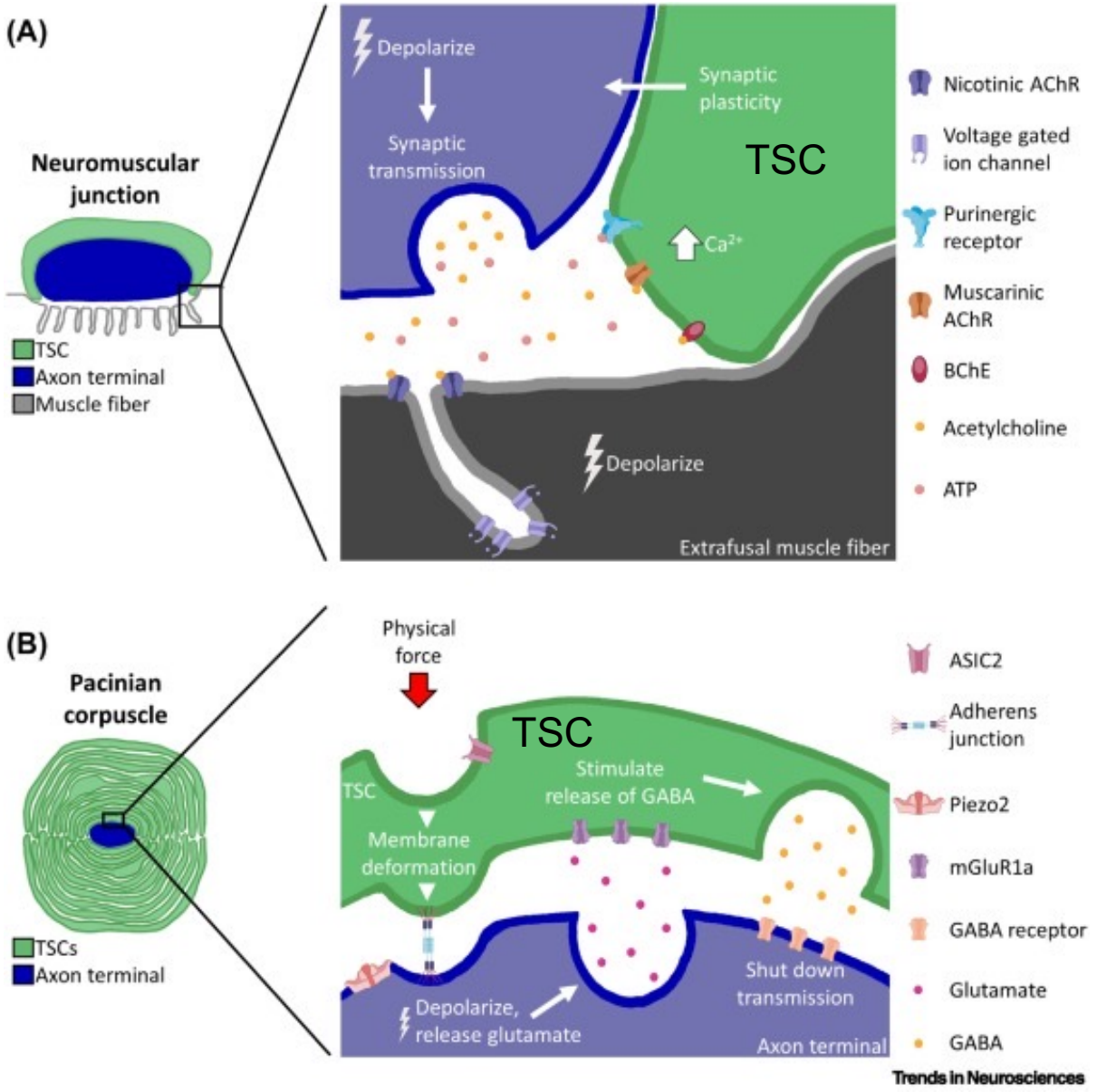

The PSCs cells are important for:

1. Synaptic transmission
2. NMJ development
3. Synaptic maintenance
4. Synaptic regeneration

The number of PSC
is correlated
with the endplate size

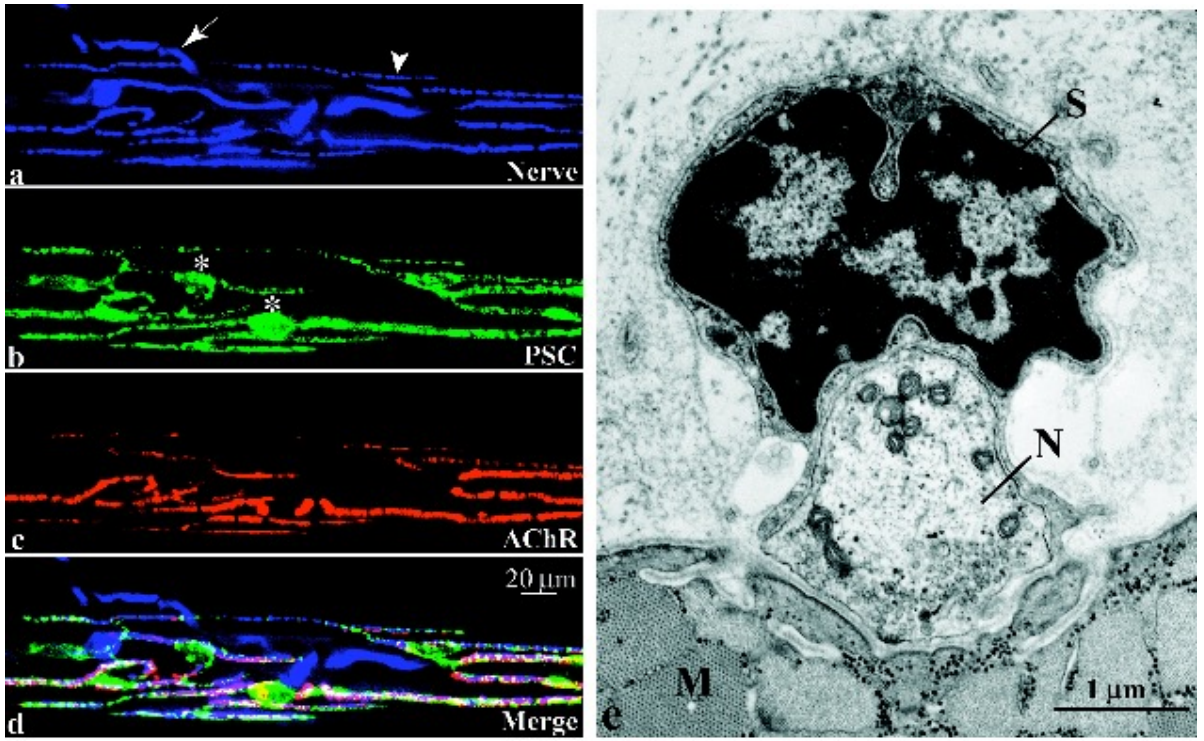

Fig. 1. The presynaptic, glial, and postsynaptic elements of the neuromuscular junction (NMJ). a-d, An adult frog neuromuscular junction labeled with antineurofilament and antisynapsin I antibodies (a) to visualize nerves, including preterminal axons (arrow in a) and nerve terminals (arrowhead in a); with a monoclonal antibody, mAb 2A12 (b), which selectively binds the surface membrane of perisynaptic Schwann cells (PSCs) in vivo (asterisks in b mark PSC cell bodies); and with α-bungarotoxin (α-BTX) (c) to visualize acetylcholine receptors (AChRs) on the postsynaptic muscle fiber. As seen in the merged image (d), the three components of the NMJ— nerve terminals, PSCs, and AChRs—are closely aligned with one another. e, Electron micrograph of an adult NMJ in cross section. The PSC (S), in this case with a densely stained nucleus, tightly covers the nerve terminal (N), which is apposed to postjunctional folds on the muscle fiber (M). (Fig. 1e adapted from Reddy and others 2003.)

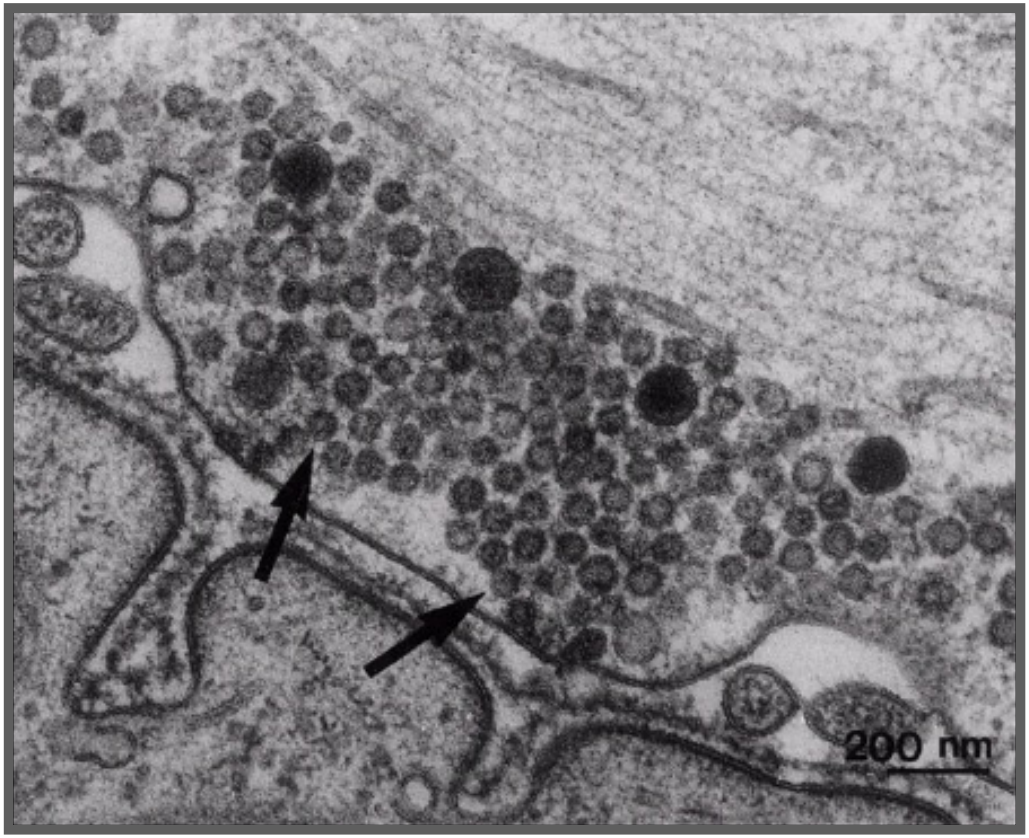

small clear vesicles:

- ACh
- ATP (Ado)

dense-core vesicles:

- substance P (SP)
- calcitonin gene-related peptide (CGRP)

Table 1. Perisynaptic Schwann cell responses to synaptic activity.

	Physiological effect on perisynaptic Schwann cells	*Methods*	*References*
Frog NMJ			
Nerve stimulation	$[Ca^{2+}]_i$ increase elicited by transmitter release	Ca^{2+} imaging	Jahromi *et al.* (1992) and Reist and Smith (1992)
Acetylcholine	Activation of muscarinic AChRs, increase of $[Ca^{2+}]_i$	Ca^{2+} imaging	Jahromi *et al.* (1992) and Robitaille (1997)
	Downregulation of GFAP expression	GFAP immunostaining	Georgiou *et al.* (1994, 1999)
ATP	Activation of P2X, P2Y, increase of $[Ca^{2+}]_i$	Ca^{2+} imaging	Jahromi *et al.* (1992) and Robitaille (1995)
Substance P	Activation of NK1 receptors, increase of $[Ca^{2+}]_i$	Ca^{2+} imaging	Bourque and Robitaille (1998)
Deprivation of synaptic activity	Increase of GFAP expression	GFAP immunostaining	Georgiou *et al.* (1994, 1999)
Mouse NMJ			
Acetylcholine	Activation of muscarinic AChRs, increase of $[Ca^{2+}]_I$	Ca^{2+} imaging	Rochon *et al.* (2001)
Adenosine	Activation of A1 receptors, increase of $[Ca^{2+}]_i$	Ca^{2+} imaging	Rochon *et al.* (2001)

The PSC receptors:

- **muscarinic ACh receptors (mAChRs)**

they are activated by the release of neurotransmitter from the nerve terminal

- **P2X and P2Y receptors (P2XRs, P2YRs)**

they are activated by the release of ATP from the nerve terminal

- **A1 adenosine receptors (ARs)**
- **NK1 receptor** (ligand: substance P)
- **nAChR** (ACh spillover)

Moreover they have butyrylcholinesterase (BChE)

- Video tripartite NMJ

PSCs are involved in synaptic activity

1. Low frequency stimulation (< 0.2 Hz) does not simulate Schwann cells
2. High frequency stimulation (40 Hz) increases the intracellular calcim concentration of Schwann cells

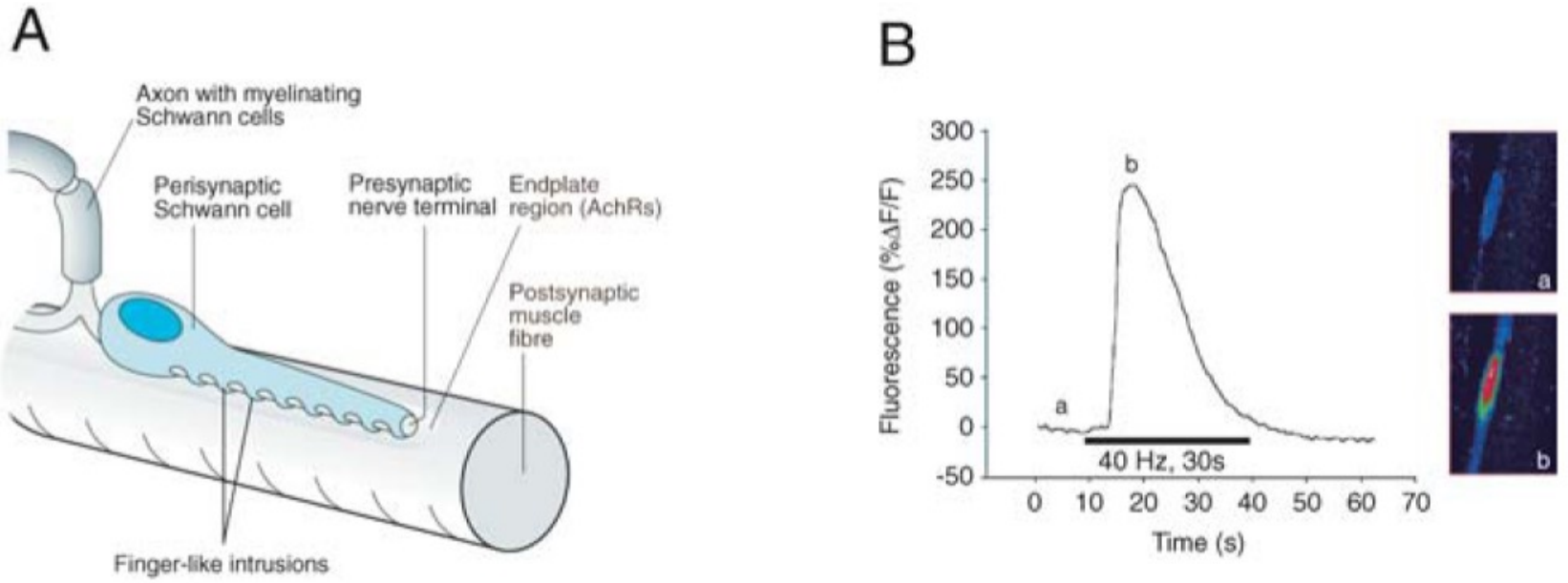

Fig. 1. Perisynaptic Schwann cells at the frog neuromuscular junction and theirCa2+response to synaptic activity. (A) PSCs, non-myelinating glial cells located at the NMJ, are closely apposed to nerve terminals and extend intermittent finger-likeintrusions into the synaptic cleft. These intrusions are located near nerve terminal active zones, where synaptic vesicles are concentrated. Thus, PSCs are well placed anatomically to interact with neurotransmission. (B) A typical PSC Ca2+ response to high-frequency motor nerve stimulation at the frog NMJ. Intracellular fluorescence changes were monitored using the Ca2+ indicator Fluo3-AM. Nerve stimulation at 0.2 Hz did not elicit a PSC Ca2+ increase, whereas stimulation at 40 Hz for 30 sec elicited a robust increase. Insert a. shows a false color confocal image of a PSC at rest. Insert b. shows the same PSC at the peak of the Ca2+ response accompanying 40 Hz stimulation. Blue represents low levels of fluorescence. and red high levels. Insert a. and b. depict the same cell as in the graph.

PSCs detect synaptic transmission

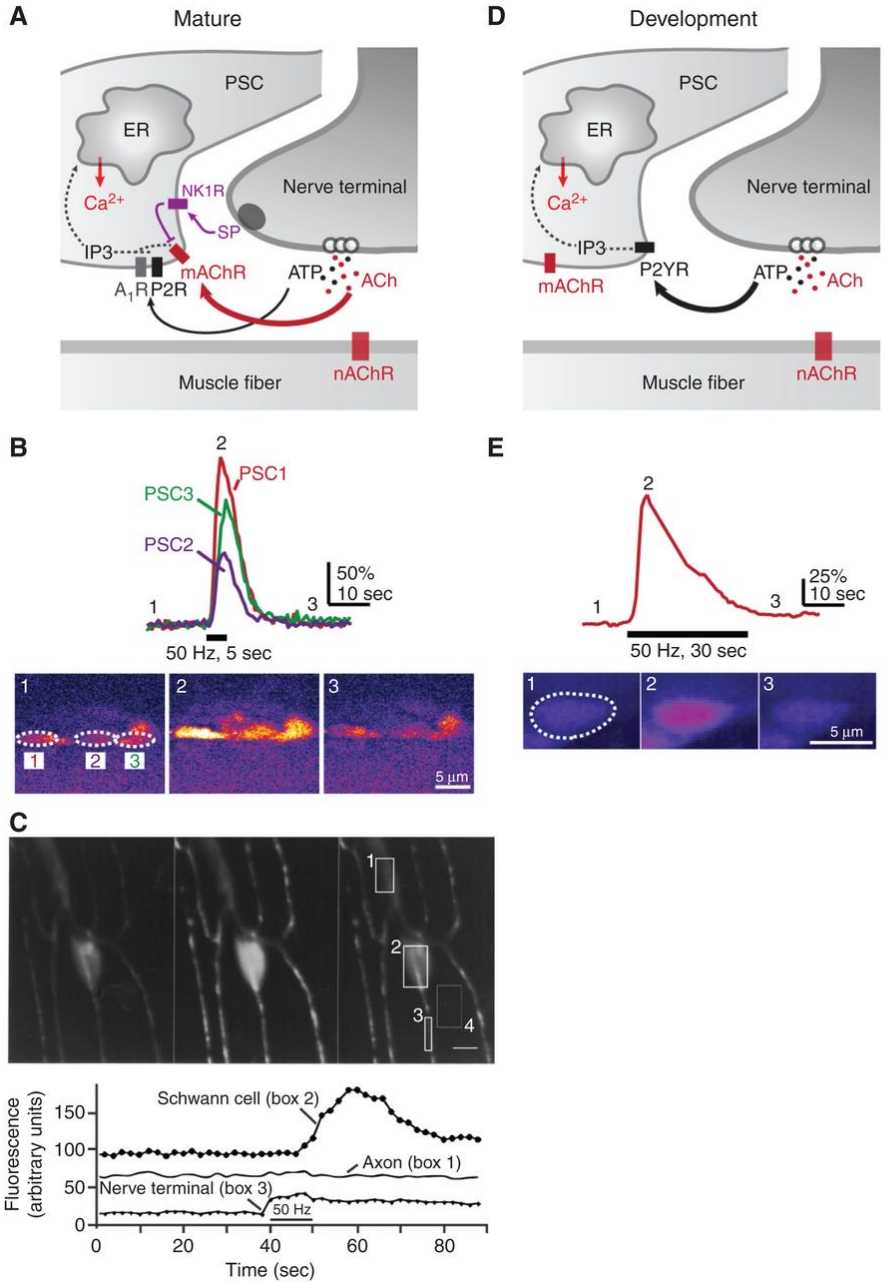

PSCs detect synaptic transmission. (*A*) Diagram depicting the receptors and their actions by which PSCs detect synaptic transmission at mature NMJ and the main regulatory mechanisms. (*B*) (*Top*) Changes in fluorescence of a Ca^{2+} indicator in PSCs of a mature mouse NMJ before, during, and after motor nerve stimulation. (*Bottom*) False color confocal images of the PSCs loaded with a Ca^{2+} indicator and from which the traces have been measured. (*C*) Images of an amphibian neuromuscular preparation showing the changes in fluorescence observed in the axonal compartment (1), the soma of a PSC (2), and the presynaptic terminal area (3) before, during, and after motor nerve stimulation (bar). (*D*) Diagram depicting the receptors and their actions by which PSCs detect synaptic transmission at developing NMJ. (*E*) (*Top*) Changes in fluorescence of a Ca^{2+} indicator in a PSC of an immature (P7) mouse NMJ before, during, and after motor nerve stimulation. (*Bottom*) False color confocal images of the PSCs loaded with a Ca^{2+} indicator and from which the traces have been measured. (Panel *C* from Reist and Smith 1992; reprinted, with permission, from the National Academy of Sciences.)

PSCs decode synaptic information

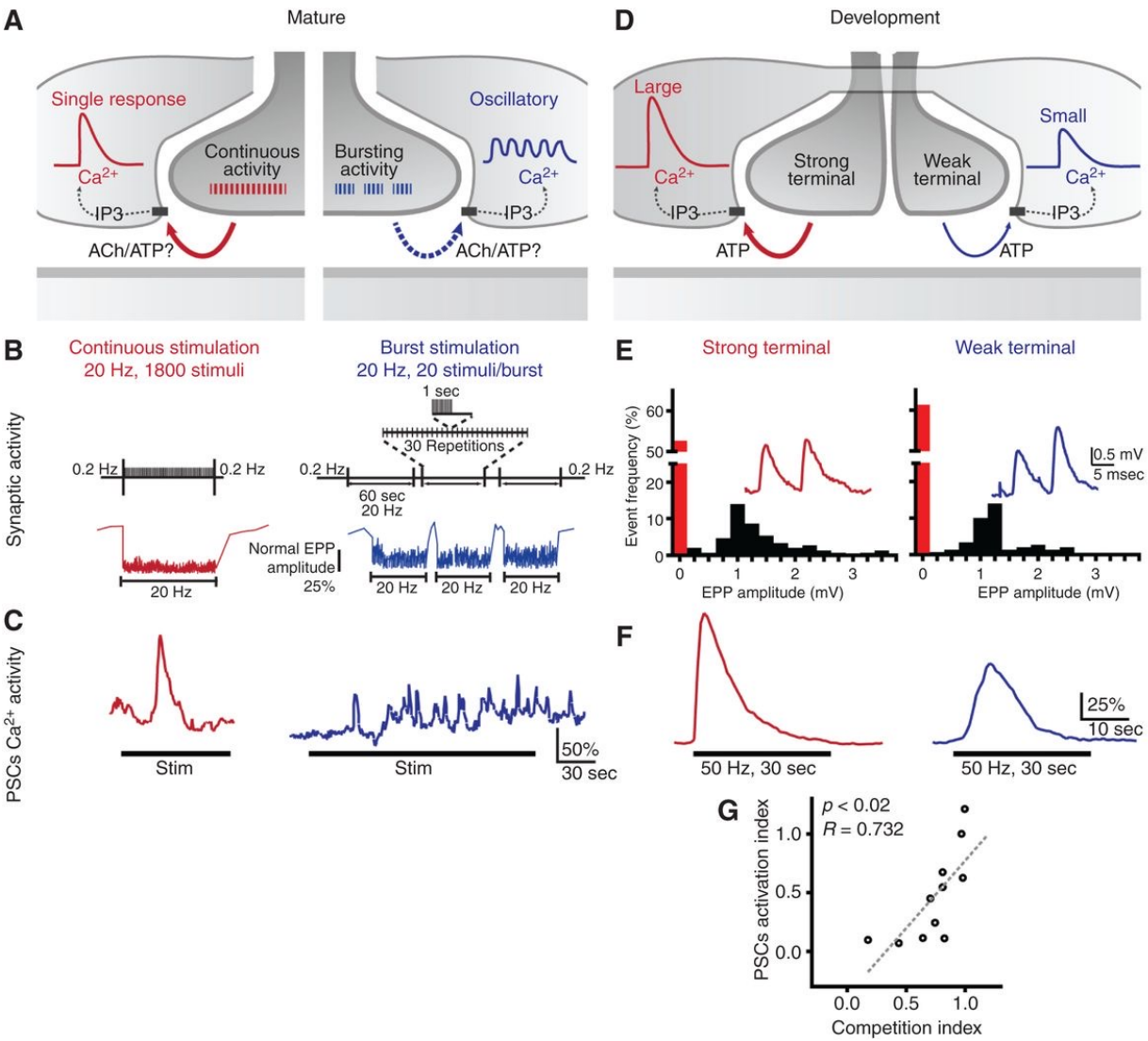

PSCs decode synaptic information. (*A*) Diagram depicting the Ca^{2+} responses in PSCs and the mechanisms involved when motor nerve activity is induced using two different patterns of stimulation (continuous or bursting activity) at mouse mature NMJs. (*B*) The bursting pattern consisting of 30 repetitions of 20 pulses at 20 Hz repeated every 2 sec and a continuous pattern of stimulation at 20 Hz for 90 sec. (*C*) Typical Ca^{2+} responses elicited by the bursting and the continuous motor nerve stimulation illustrated in *B*. Note the difference in the kinetics of the Ca^{2+} responses revealing the ability of PSCs to decode the pattern of synaptic activity. (*D*) Diagram depicting the Ca^{2+} responses in PSCs elicited by independent activity of competing nerve terminals (weak and strong) at NMJs during synapse formation. (*E*) Quantal analysis based on the failure rates of two competing inputs at an immature NMJ. Note the larger percentage of failures of the weak nerve terminal. (*F*) Independent Ca^{2+} responses in the PSC that covers the same two terminals (weak and strong) in *E*. Note the difference in the amplitude of the two responses, the stronger terminal eliciting a larger Ca^{2+} response. (*G*) A PSC activation index as a function of the synaptic strength index showing a continuum in the amplitude of Ca^{2+} responses as a function of the relative strength of competing nerve terminals. These results indicate that a single PSC can decipher the strength of nerve terminals competing for the territory at a same NMJ. (Panels *B* and *C* from data in Todd et al. 2010; and panels *E*–*G* from data in Darabid et al. 2013.)

PSCs in short-term plasticity

depression

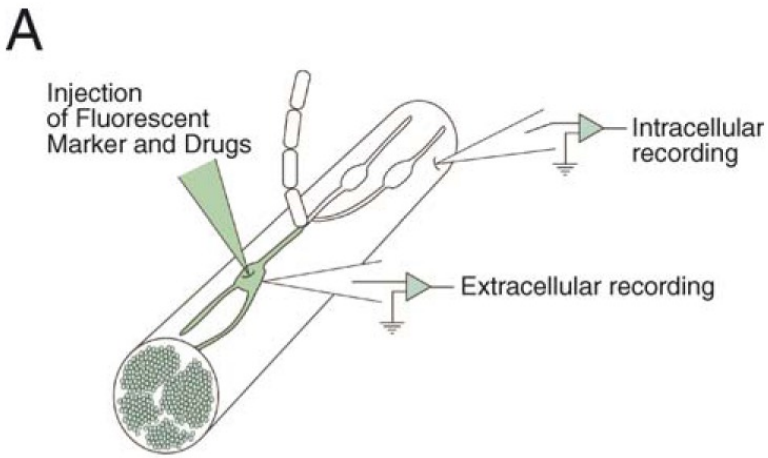

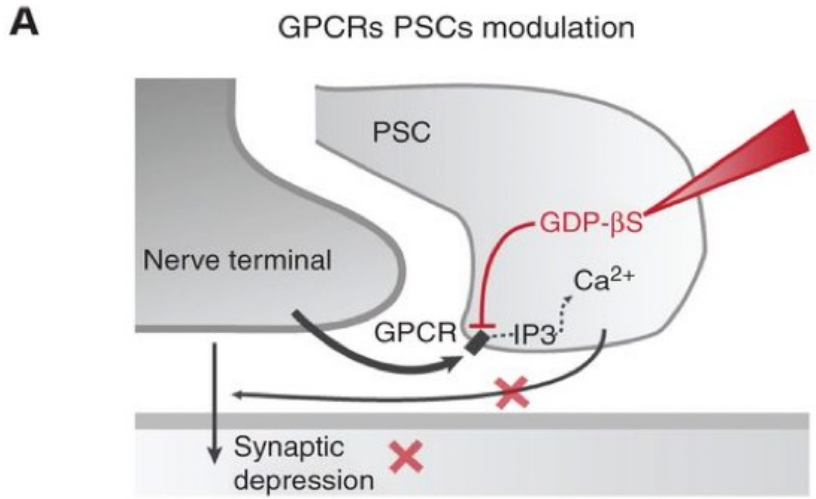

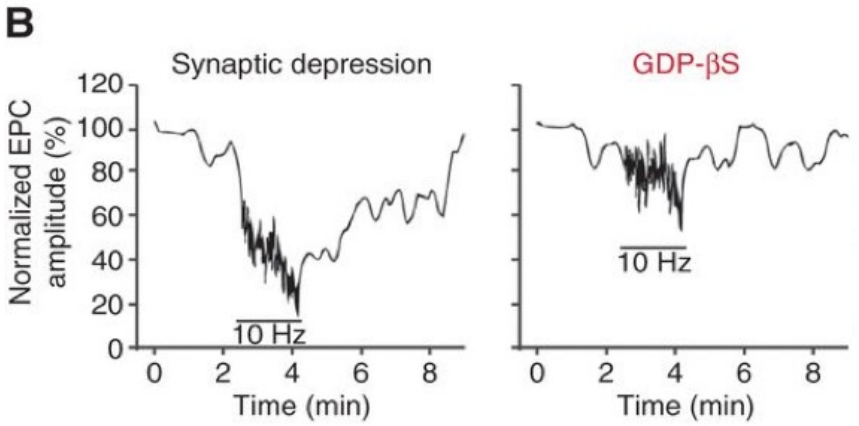

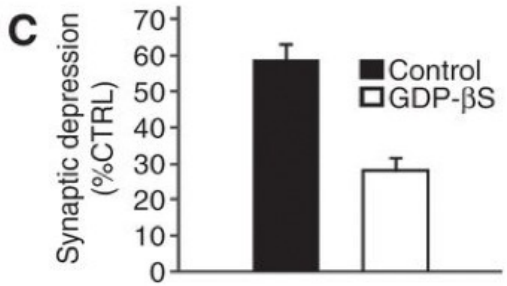

PSCs in short-term plasticity

depression and potentation

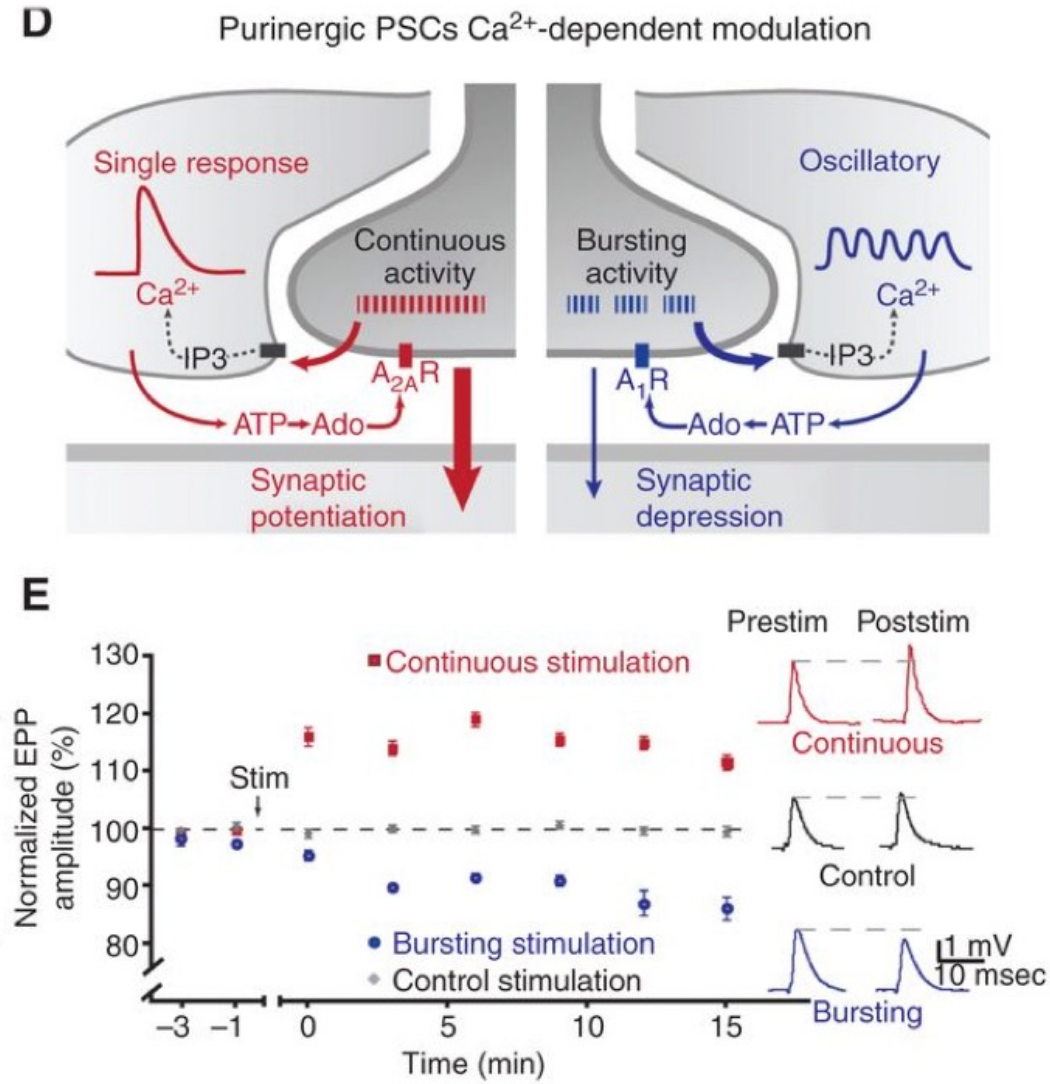

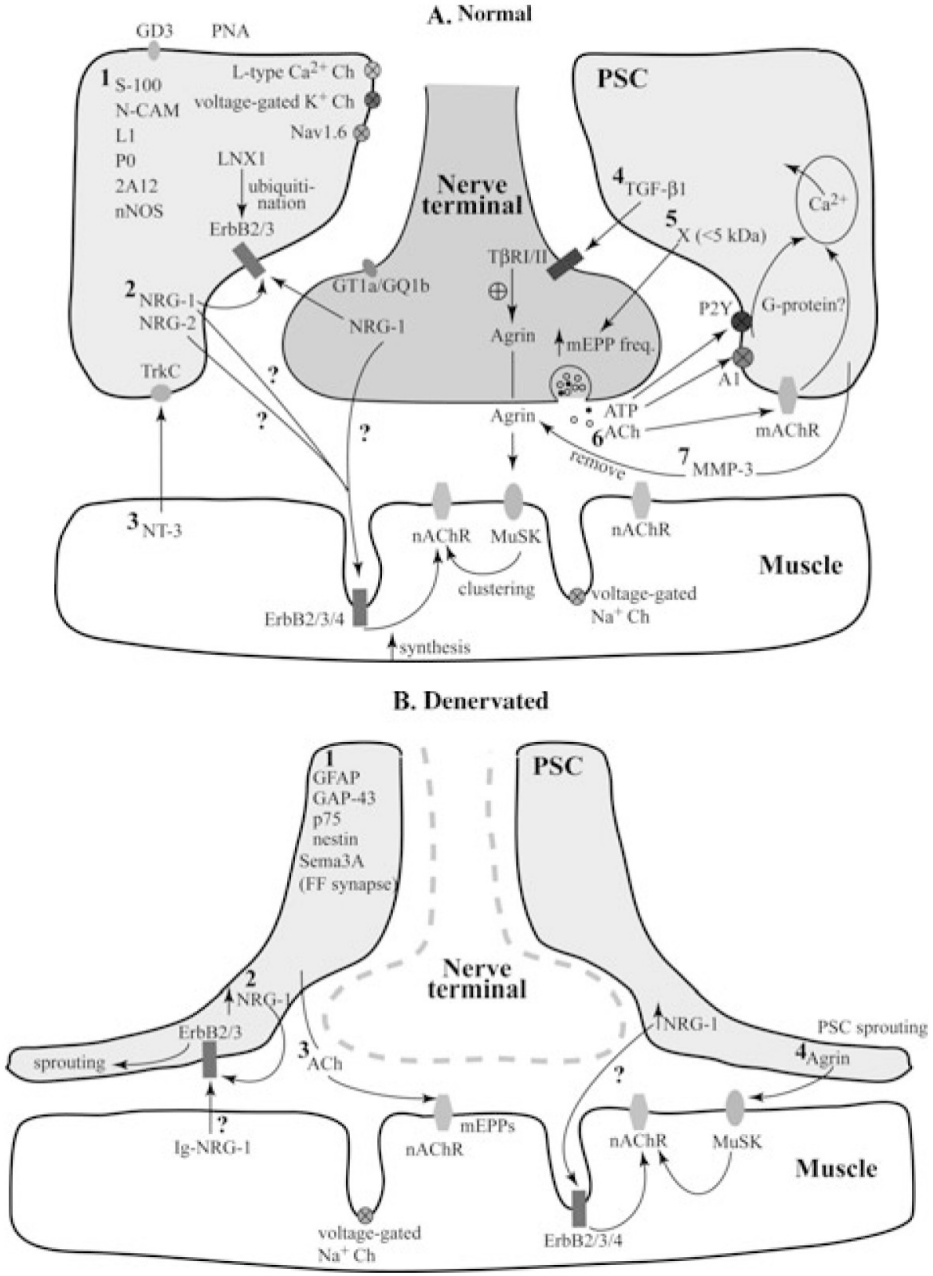

FIGURE 1. (**A**) A schematic diagram depicting some of the interactions between PSCs and nerve–muscle contacts in intact muscles. ***1***. PSCs express a variety of molecules, including S100, N-CAM, L1, and myelin-associated protein P0. Frog PSCs also express unknown molecules recognized by mAb 2A12. In addition, several ion channels, such as L-type calcium channel, voltage-gated potassium channel, and voltage-gated sodium channels Nav1.6, have been shown to be localized on PSCs. ***2***. PSCs also express neuregulin (NRG)-1, NRG-2, and their receptors ErbB2/3. Nerve-derived NRG-1 is required for the survival of developing PSCs. NRG-1 and NRG-2 derived from PSCs, together with NRG-1 derived from the nerve terminal, may play a role in regulating the synthesis of nicotinic acetylcholine receptors (nAChRs) in postsynaptic muscle fibers. ***3***. NT-3 receptor TrkC is localized on PSCs. Muscle-derived NT-3 may be a survival or mitogenic factor for developing PSCs. ***4***. Schwann cell–derived molecules, one of which has been suggested to be transforming growth factor (TGF)-β1, enhance synaptogenesis via upregulating the expression of neuronal agrin during development. ***5***. Unknown factor(s) (molecular weight <5 kDa) released from Schwann cells potentiate(s) spontaneous synaptic activity during development. ***6***. Synaptic activity increases intracellular calcium level in PSCs via activating muscarinic AChRs (mAChRs) by ACh or P2Y and A1 receptors by ATP. ***7***. PSCs may release and activate matrix metalloproteinase 3 (MMP3), which may be involved in removing agrin from synaptic basal lamina. (**B**) A schematic diagram depicting some of the interactions between PSCs and nerve–muscle contacts in denervated muscles. ***1***. The expressions of several molecules are upregulated in PSCs after denervation, including GFAP, GAP-43, p75, nestin, and Semaphorin (Sema) 3A (only at fast-fatigable synapses). ***2***. Upregulated NRG-1 in PSCs may play a role in inducing PSC sprouting upon denervation. ***3***. ACh, released from PSCs, can induce spontaneous synaptic activity at denervated NMJs. ***4***. PSC-derived agrin may play a role in inducing AChR clusters underneath PSC sprouts in denervated muscles.

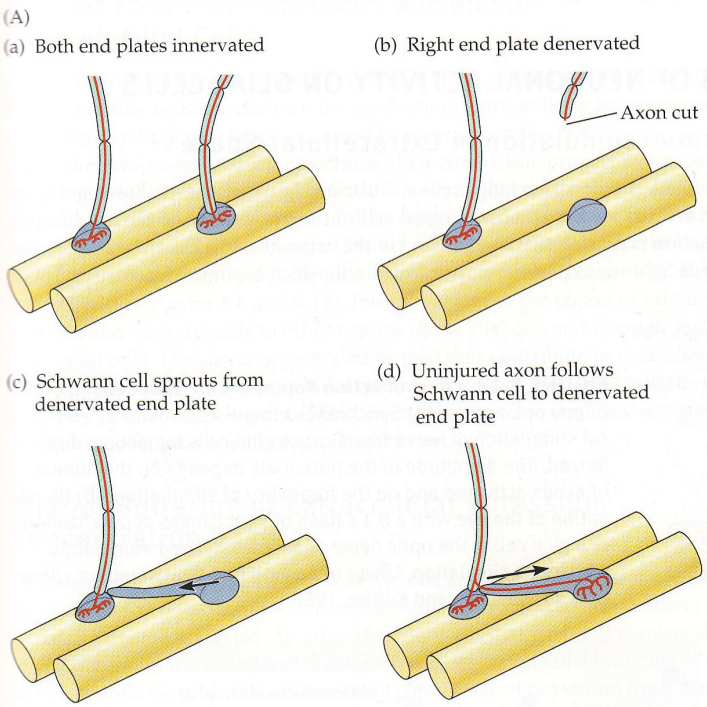

FIGURE 8.12 Role of Schwann Cells in Guiding Axons to denervated motor end plates of skeletal muscle fibers. (A) Schematic representation of the effects of partial denervation of a rat muscle. (a) At normal nerve–muscle synapses, an axon and its Schwann cell (shown in blue) are closely apposed. (b) The axon innervating the right-hand muscle fiber is cut, leading to degeneration of the nerve terminal. (c) In response to this denervation, the terminal Schwann cells on the denervated muscle fiber (blue) grow processes, one of which reaches the nerve terminal at the adjoining muscle fiber. (d) An axonal sprout is induced from the uninjured nerve terminal. It grows along the Schwann cell process to the denervated end plate, which it reinnervates. (B) Growth of axonal sprouts (labeled with antineurofilament antibody) to denervated synapses along processes extended by Schwann cells (labeled with a monoclonal antibody, 4E2, which is specific for Schwann cell bodies and processes). Three days after partial denervation, a neurofilament-labeled nerve sprout has grown from the innervated junction (red) to a denervated junction (blue) by following the Schwann cell process that had grown earlier. The innervated and denervated motor end plates were identified by the patterns of staining of axons and Schwann cells. (After Son and Thompson, 1995; micrographs kindly provided by W. Thompson.)

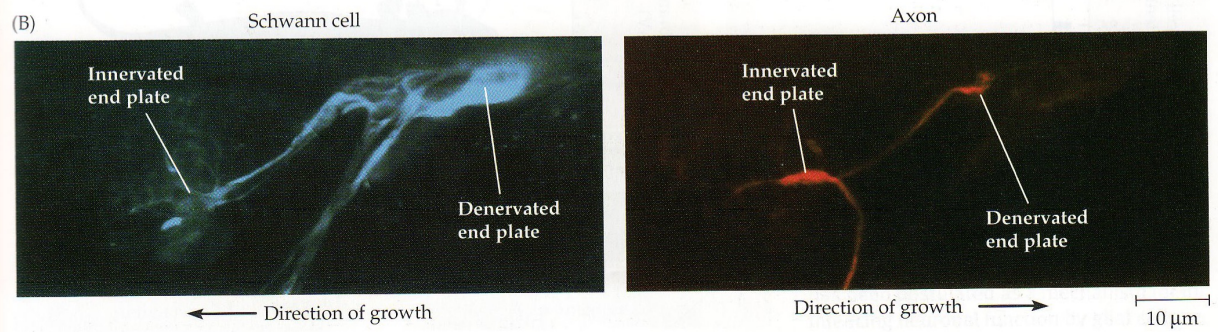

PSCs: stability, efficacy, plasticity and repair of the NMJ

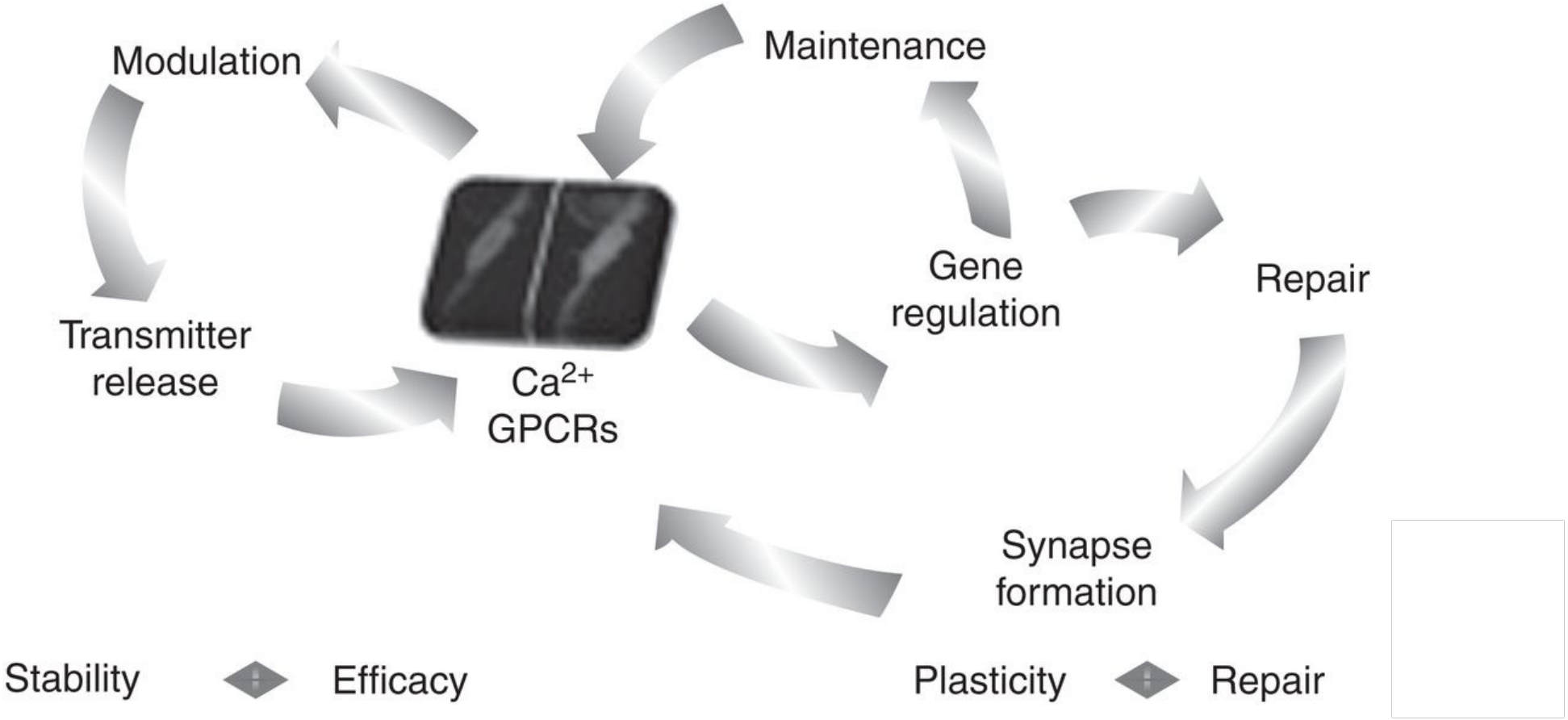

balance between **Muscarinic** *vs* **Purinergic** receptors